Biophysical Insight into Furosemide Binding to Human Serum Albumin: A Study To Unveil Its Impaired Albumin Binding in Uremia

ARTICLE *in* THE JOURNAL OF PHYSICAL CHEMISTRY B · MARCH 2013

Impact Factor: 3.3 · DOI: 10.1021/jp3069877 · Source: PubMed

THE JOURNAL OF PHYSICAL CHEMISTRY B

Article

pubs.acs.org/JPCB

Biophysical Insight into Furosemide Binding to Human Serum Albumin: A Study To Unveil Its Impaired Albumin Binding in Uremia

Nida Zaidi,[†] Ejaz Ahmad,[†] Mohd Rehan,[‡] Gulam Rabbani,[†] Mohammad R. Ajmal,[†] Yusra Zaidi,[§] Naidu Subbarao,[‡] and Rizwan H. Khan*[,†]

[†]Interdisciplinary Biotechnology Unit, Aligarh Muslim University, Aligarh 202002, India

[‡]School of Computational and Integrative Sciences, Jawaharlal Nehru University, New Delhi 110062, India

[§]Department of Zoology, Aligarh Muslim University, Aligarh 202002, India

Supporting Information

ABSTRACT: Exogenous substances like drugs, when absorbed, enter into the circulatory system and bind reversibly and extensively to human serum albumin (HSA). But transport of various drugs like a diuretic, furosemide (FUR), via albumin in uremia is seriously compromised due to accumulation of uremic toxins. The reason behind it is explored by investigating the binding mechanism of FUR to HSA. Isothermal titration calorimetry results show that FUR binds with HSA at high ($K_b \sim 10^4$) and low affinity ($K_b \sim 10^3$) sites whereas spectroscopic results predict binding at a single site ($K_b \sim 10^5$). Thermodynamic analysis shows that the HSA-FUR complex formation occurs via hydrogen bonds and hydrophobic interactions and undergoes slight structural changes, as evident by FTIR and far-UV CD. Further, the lifetime of HSA decreases only marginally and thus the magnitude of energy transfer efficiency is small, as obtained by time-resolved measurements. A displacement experiment predicts that the FUR binds mainly to site I but a new site having lower affinity is also observed, which shares some residues with site II as supported by molecular docking results. Results revealed that in uremia, FUR indirectly competes for Arg410, Lys414, and Ser489 with site II bound uremic toxins and directly competes for site I with site I bound uremic toxins.

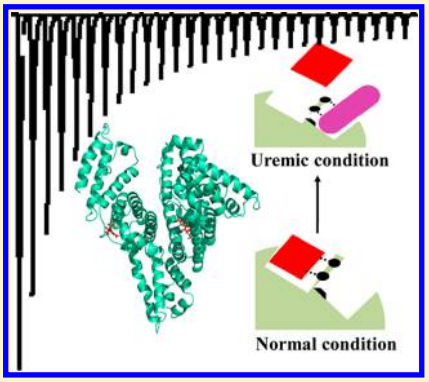

1. INTRODUCTION

Human serum albumin (HSA) is a main carrier for a variety of endogenous and exogenous substances in the body and also plays a key role in maintaining normal osmolarity in plasma and in interstitial fluid.[1−3] It is a single chain nonglycosylated polypeptide of 66.5 kDa. The protein has three homologous domains (I−III), each domain comprises two subdomains (A and B) that possess common structural elements.[4,5] As of its transporting role, it binds substances at two major binding regions, namely Sudlow's site I and II, which are located within cavities in subdomains IIA and IIIA, respectively.[6] Generally, upon absorption exogenous substances like drugs enter into the circulatory system and bind reversibly to serum albumin, which assists in their distribution and deposition.[7,8] But, transport of various drugs via albumin in a pathological ill condition like uremia, is seriously compromised.[9,10] Among them, binding of furosemide (FUR), a diuretic drug, is most adversely impaired, which normally binds 99% to albumin at its total concentration of 10 μg mL^{-1}.[11,12] Hence, a decrease in the protein bound fraction of FUR may affect the pharmacokinetics of the drug, which includes its tubular secretion and increased metabolic clearance in uremic patients.[13] Although the molecular mechanism underlying impaired albumin FUR binding in uremic conditions is poorly understood, two major reasons have been suggested. First, it may be due to some conformational changes in albumin under chronic renal disease but putative structural modifications of pathological HSA have been disputed for decades.[14−16] Second, according to the most accepted hypothesis, HSA binding sites might be occupied by uremic toxins, viz. hippuric acid (HA), indoxyl sulfate (IS), 3-carboxy-4-methyl-5-propyl-2-furanpropionic acid (CMPF), indole-3 acetic acid (IAA), etc.[17] However, from the available literature, it is found that FUR binds to site I of HSA[11,16,18] whereas all predominant uremic toxins except CMPF bind mainly to site II of HSA.[19−21] So, only CMPF is the uremic toxin that directly inhibits the binding of FUR to albumin as they share the same binding site. But, the reason behind inhibition by site II bound uremic toxins of FUR binding to albumin is still unclear. Thus, to elucidate the plausible reason behind impaired albumin binding of FUR, energetic and binding parameters along with the location of FUR binding sites on albumin are determined by fluorescence spectroscopy (steady state and time-resolved), ITC, FRET, esterase activity of HSA, and molecular docking and then the binding site location is correlated with the binding sites of uremic toxins available in the literature. Further, secondary structural changes

Received: July 14, 2012
Revised: January 28, 2013

   dx.doi.org/10.1021/jp3069877 | J. Phys. Chem. B XXXX, XXX, XXX−XXX

on the binding of FUR to HSA are monitored by circular dichroism and Fourier transform infrared spectroscopy. This study is the first to utilize ITC, FRET, activity assay, and molecular docking to obtain the binding parameters, energetics, and structural information for binding of FUR to human serum albumin.

2. EXPERIMENTAL SECTION

2.1. Materials and Sample Preparation. Human serum albumin (A1887; essentially globulin and fatty acid free), furosemide (F4381), warfarin (A2250), phenylbutazone (P8386), and *p*-nitrophenyl acetate (N8130) were procured from Sigma Aldrich. Diazepam was the product of Ranbaxy Laboratories Ltd. All other reagents were of analytical grade. HSA and drug solutions were prepared in 20 mM sodium phosphate buffer (pH 7.4). The protein was dialyzed and its concentration was estimated spectrophotometerically using $E^{1\%}_{280nm}$ = 5.3. All drug solutions were prepared by weight/volume (w/v).

2.2. Steady State Measurements. Steady state absorption measurements were carried out on a Perkin-Elmer Lambda 25 double beam UV−vis spectrophotometer attached with Peltier temperature programmer-1 (PTP-1). All the steady state fluorescence measurements were recorded on Shimadzu 5301PC fluorescence spectrophotometer equipped with water circulator (Julabo Eyela). For fluorescence quenching measurements, HSA (5 μM) was titrated with varying concentrations of FUR (0−11 μM) at 25, 30, and 37 °C. These samples were excited at 295 nm, and the fluorescence emission was collected from 310 to 410 nm. However, for steady state FRET measurements, the fluorescence emission was collected from 300 to 500 nm. The excitation and emission slits were set at 3 nm. Respective blanks were subtracted. The fluorescence intensity was corrected for inner filter effects of protein and ligand using the equation:[22]

$$F_{cor} = F_{obs} D_f 10^{(A_{295nm}+A_{340nm})/2} \quad (1)$$

where F_{cor} and F_{obs} are the corrected and observed fluorescence intensities, D_f is the dilution factor, and A_{295nm} and A_{340nm} are the sum of the absorbance of protein and ligand at the excitation (295 nm) and emission (340 nm) wavelengths, respectively. The average of A_{295nm} and A_{340nm} for HSA and FUR lay in the range from 0.02 to 0.07.

2.3. Time-Resolved Fluorescence Measurements. Fluorescence lifetime measurements were performed using the time-correlated single photon counting (TCSPC) model 5000 U (Horiba Jobin Yvon). The samples were excited at 295 nm using a NanoLED pulsed laser. The instrument response function (IRF) was obtained using LudoxTM suspension. The full width at half-maxima (fwhm) of the IRF was 750 ps. The emission decay data at 340 nm were analyzed using the software, DAS6, provided with the instrument.

2.4. Isothermal Titration Calorimetric Measurements (ITC). The energetics of the binding of FUR to HSA at 25, 30, and 37 °C were measured using a VP-ITC titration microcalorimeter (MicroCal Inc., Northampton, MA). Prior to the titration experiment, all samples were degassed properly on a thermovac. The sample and reference cell of the calorimeter were loaded with HSA solution (18 μM) and 20 mM sodium phosphate buffer (pH 7.4), respectively. Then multiple injections of 10 μL of FUR solution (1.285 mM) were made into the sample cell containing HSA. Each injection was made over 20 s with an interval of 180 s between successive injections. The reference power and stirring speed were set at 16 μcal^{-1} and 307 rpm, respectively. Heats of dilution for the ligands were determined in control experiments, and these were subtracted from the integrated data before curve fitting.

2.5. Circular Dichroism Spectroscopic Measurements. The far-UV CD spectra of HSA (5 μM) were collected in the presence of FUR at molar ratio of 1:0, 1:1, and 1:2 in a JASCO-J815 spectropolarimeter equipped with a Peltier-type temperature controller at 25, 30, and 37 °C. Spectra were collected from 200 to 250 nm with 20 nm/min scan speed and a response time of 2 s. Respective blanks were subtracted.

2.6. FTIR Spectroscopic Measurements. Spectra of HSA in the presence and absence of drug were collected on a Nicolet 6700 FTIR spectrophotometer (DTGS detector, Ni-chrome source and KBr beamsplitter) from 1700 to 1600 cm^{-1} using a ZnSe window at room temperature. For each spectrum, 256 scans were averaged with a resolution of 4 cm^{-1}. The drug with HSA was incubated for 1 h prior to scanning. Respective blanks were subtracted. The curve fitting was done by assuming mixed Lorentzian−Gaussian line shape function. The curve fitting, smoothing, baselines correction, and area calculation were carried out using the built-in software (OMNIC version). The resulting fitted curve was analyzed by taking into account the band assignment for the secondary structure previously reported in the literature[23] α-helix (1648−1657 cm^{-1}), β-sheet (1623−1641 cm^{-1}), turn (1662−1686 cm^{-1}), random coil (1642−1657 cm^{-1}), and β-antiparallel (1674−1696 cm^{-1}).

2.7. Effect of Drug Binding on Esterase Activity of HSA. Drug site II of HSA possessed a well-known esterase-like activity toward *p*-nitrophenyl acetate (*p*-NPA).[24] Thus the reaction of *p*-NPA with HSA in the absence and presence of drug (i.e., 0−45 μM) was followed at 405 nm by monitoring the appearance of yellow product *p*-nitrophenol for 1 min at 25 °C. The molar extinction coefficient of *p*-nitrophenol was taken as 17800 M^{-1} cm^{-1}. The reaction mixture contained 15 μM HSA whereas *p*-NPA varied from 0 to 600 μM in 20 mM sodium phosphate buffer (pH 7.4). The control (in the absence of HSA) was also taken into consideration.

2.8. Molecular Docking. The crystal structure of HSA (PDB: 1AO6) was retrieved from the Protein Data Bank on which addition of hydrogen atoms was done followed by minimization and optimization using the OPLS 2005 force field in the premin option of Schrödinger GLIDE in the Schrödinger protein preparation wizard. The grids were generated and cover all the residues in a 5 Å neighborhood of the PBZ and WAR for site I and DIA for site II. The FUR molecule was then prepared in the Schrödinger ligprep wizard and predocking preparations were done as that for protein. Docking was then performed using GLIDE and its output G score was calculated as[25]

$$\text{G score} = \text{H bond} + \text{eLipo} + \text{metal} + \text{site} + 0.13\text{Coul} + 0.065\text{vdW} - \text{BuryP} - \text{RotB} \quad (2)$$

where H bond = hydrogen bonds, Lipo = hydrophobic interactions, metal = metal-binding term, site = polar interactions in the binding site, vdW = van der Waals forces, Coul = Columbic forces, BuryP = penalty for buried polar group, RotB = freezing rotable bonds.

X-Score v1.2.1 was used to calculate negative logarithm of dissociation constant of the ligand to the protein, $-\log(K_d)$, and binding energy (kcal mol^{-1}). X-Score was reported to have an accuracy of ±2.2 kcal mol^{-1} to the actual binding energies.

dx.doi.org/10.1021/jp3069877 | J. Phys. Chem. B XXXX, XXX, XXX−XXX

The Ligplot program and PyMOL were used for analyzation and visualization of the interaction of docked protein−ligand complex, respectively.

3. RESULTS AND DISCUSSION

3.1. Steady State Fluorescence Results. Tryptophan, tyrosine, and phenylalanine are the three aromatic fluorophores that are used for studying conformational changes on drug binding. However, among them, the contribution of tryptophan is maximum.[26] Fluorescence quenching of aromatic fluorophores in HSA by FUR at three different temperatures viz. 25, 30, and 37 °C is evaluated in the presence of varying concentrations of FUR. As shown in Figure 1, HSA has the strong emission peak at 340 nm on excitation at 295 nm, which decreases with gradual addition of FUR at all three temperatures.[27,28] However, the quenching of Trp fluorescence emission is a maximum at 25 °C and minimum at 37 °C.

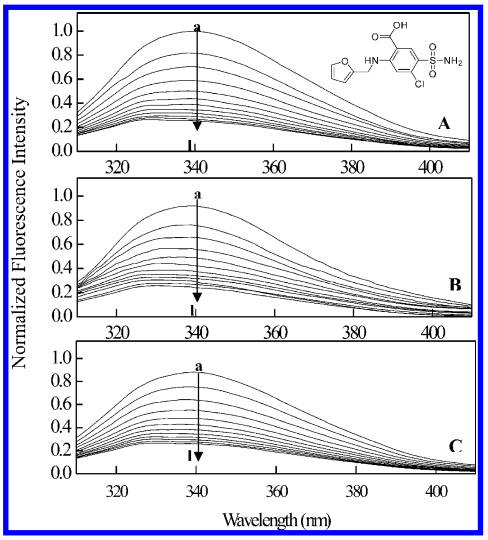

Figure 1. Normalized fluorescence emission spectra of HSA in the presence of different concentrations of FUR at (A) 25 °C, (B) 30 °C, and (C) 37 °C. a−l: 0−11 μM of FUR at increments of 1 μM. The inset corresponds to the molecular structure of FUR.

3.1.1. Binding Affinity. To obtain the Stern−Volmer quenching constant (K_{sv}) and binding constant (K_b), the fluorescence quenching data of HSA-FUR binding at different temperatures are analyzed by the linear and modified Stern−Volmer equation, respectively:[29]

$$\frac{F_o}{F} = Ksv[Q] + 1 = kq\tau_o[Q] + 1 \quad (3)$$

$$\log\left(\frac{F_o}{F} - 1\right) = \log K_b + n \log[Q] \quad (4)$$

where F_o and F are the fluorescence intensities in the absence and presence of quencher (FUR), K_{sv} and k_q are the Stern−Volmer quenching and bimolecular rate constants, respectively, and τ_o is the average integral fluorescence lifetime of tryptophan, which is ~5.7 × 10^{-9} s. K_{sv} is calculated from the slope of plot F_o/F vs [Q], whereas the slope and intercept of plot $\log(F_o/F - 1)$ vs $\log[Q]$ give n and K_b, respectively (Figure 2A,B). As shown in Table 1, the values for binding constant are on the order of 10^5 and decrease wtih increasing temperature. This suggests static quenching phenomenon, which is also the reason behind the fall in fluorescence emission of Trp with the rise in FUR concentration.[30,31]

3.1.2.. Mechanism of Binding. Fluorescence quenching can be either dynamic or static in nature. To know about the quenching mechanism of HSA by FUR, the mechanism is assumed to be dynamic. Thus by eq 3, k_q is obtained, which lies on the order of 10^{13}, as shown in Table 1. However, the k_q for the HSA-FUR system is 1000 times lower than the maximum scatter collision quenching constant of various quenchers with biopolymers (2×10^{10} $M^{-1}s^{-1}$).[26] This shows that quenching is not initiated by dynamic diffusion but occurs by formation of a strong complex between HSA and FUR.[28] Further, the temperature dependence of K_{sv} is studied as a type of quenching and can be distinguished by the differential response toward temperature and viscosity. In static quenching, K_{sv} decreases with an increase in temperature due to the formation of complex with protein, which undergoes dissociation on increasing temperature. However, for dynamic quenching, K_{sv} increases with temperature as in this case higher temperature results in faster diffusion of quencher and hence larger extent of collisional quenching.[31] To further confirm the mechanism, time-resolved fluorescence spectroscopy have been done.

3.1.3. Mode of Binding. The signs and magnitude of change in enthalpy (ΔH), entropy (ΔS), and free energy (ΔG) for protein−drug interaction can be exploited to evaluate the main forces contributing to the formation of a protein−drug complex.[32] According to eq 5, ΔH and ΔS are obtained from

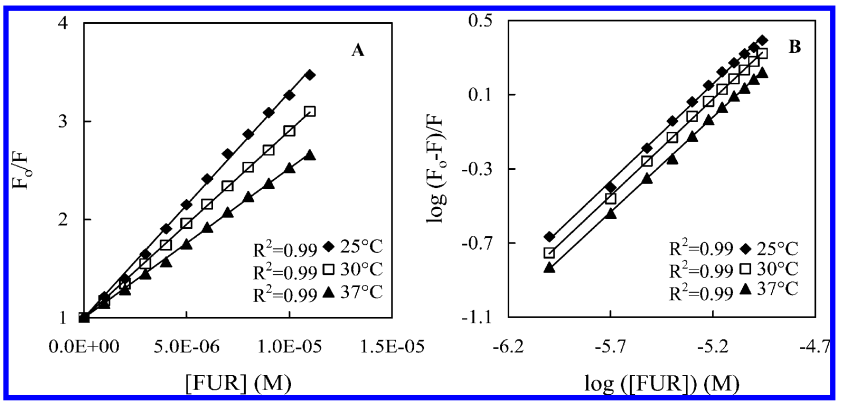

Figure 2. Stern−Volmer (A) and modified Stern−Volmer plots (B) of fluorescence quenching of HSA by FUR at different temperatures. Protein (5 μM) was excited at 295 nm.

dx.doi.org/10.1021/jp3069877 | J. Phys. Chem. B XXXX, XXX, XXX−XXX

Table 1. Binding and Thermodynamic Parameters of FUR-HSA at Different Temperatures Obtained from Fluorescence Quenching Experiments[a]

temp (°C)	n	K_{sv} (M^{-1})	K_b (M^{-1})	k_q (M^{-1} s^{-1})	ΔH (kcal mol^{-1})	$T\Delta S$ (kcal mol^{-1})	ΔG (kcal mol^{-1})
25	1.05	2.29×10^5	4.09×10^5	4.01×10^{13}		−3.41	−7.65
30	1.05	1.90×10^5	3.13×10^5	3.33×10^{13}	−11.07	−3.47	−7.61
37	1.03	1.52×10^5	1.99×10^5	2.66×10^{13}		−3.55	−7.51

[a] R^2 for all values ranges from 0.98 to 0.99.

the slope and intercept of a linear van't Hoff plot between ln K_b vs $1/T$ (not shown):

$$\ln K_b = -\frac{\Delta H}{RT} + \frac{\Delta S}{R} \tag{5}$$

and the change in free energy (ΔG) is calculated from the Gibbs−Helmholtz equation:

$$\Delta G = -RT \ln K_b \tag{6}$$

where R (1.987 cal mol^{-1} K^{-1}) is the gas constant and T is the absolute temperature (K). The calculated thermodynamic parameters ΔH, ΔS, and ΔG are summarized in Table 1. The negative ΔH and ΔG signify the exothermic and spontaneous nature of process at all studied temperatures. According to Ross and Subramanium,[32] negative ΔH and ΔS values suggest the involvement of hydrogen bonding in HSA-FUR complex formation and a decrease in entropy is attributed to the formation of hydrogen bonds between FUR and HSA. Furthermore, it is found that the major contribution to ΔG arises from ΔH rather than ΔS, so the binding process is enthalpy driven.

3.1.4. Probing Binding Site Using Site Markers. The determination of binding site location of FUR on HSA is performed by using the simple approach of competitive binding between FUR and site specific markers, viz., warfarin (WAR), phenylbutazone (PBZ) for site I and diazepam (DIA) for site II,[33,34] by keeping a constant concentration of protein and marker in the ratio of 1:1 and varying the concentration of FUR (0−11 μM). The ligands bind HSA at two major binding regions, namely Sudlow's site I and site II, which are located within specialized cavities in subdomains IIA and IIIA, respectively.[6] To probe the binding site of FUR on HSA, K_{sv} values in the absence and presence of markers are calculated by the Stern−Volmer equation and presented in Table 2. The

Table 2. Effect of Site Markers on Binding of FUR to HSA

	without the site marker	with PBZ	with WAR	with DIA
K_{sv}	2.29×10^5	5.01×10^4	1.03×10^5	1.32×10^5
R^2	0.99	0.99	0.99	0.99

values of K_{sv} for FUR decrease in the presence of PBZ and WAR (site I markers). It suggests that FUR binds to site I because in the presence of site markers having the same binding site as that of the test drug, the value of the quenching constant should decrease due to competition.[31] However, a decrease in the values of K_{sv}, for FUR in the presence of DIA (site II marker) is also not negligible, which is suggestive of binding of FUR to site II. But the decrease in K_{sv} of later is small so FUR has a low affinity for site II.

3.2. Steady State Fluorescence Resonance Energy Transfer (FRET). According to Förster nonradiation energy transfer theory, the parameters related to energy transfer can be calculated on the basis of equations as follows:[35,36] The efficiency of energy transfer (E) can be calculated as

$$E_{FRET} = \left(1 - \frac{F}{F_o}\right) = \frac{R_o^6}{R_o^6 + r^6} \tag{7}$$

where F_o and F are the fluorescence intensities of HSA in the absence and presence of drug, respectively, r is the distance between the donor and acceptor, and R_o is the distance at which transfer efficiency equals 50%, which can be calculated as

$$R_o^6 = 8.79 \times 10^{-25} K^2 n^{-4} \varphi J \tag{8}$$

where K^2 is the factor related to the geometry of the donor and acceptor of dipoles, n is the refractive index of the medium, φ is the fluorescence quantum yield of the donor in the absence of acceptor, and J is the overlap integral of donor fluorescence emission and the acceptor absorption, which can be calculated by

$$J = \frac{\int_0^\infty F(\lambda)\, \varepsilon(\lambda) \lambda^4\, d\lambda}{\int_0^\infty F(\lambda)\, d\lambda} \tag{9}$$

where $F(\lambda)$ is the fluorescence intensity of the donor at wavelength range λ, which is dimensionless, and $\varepsilon(\lambda)$ is the molar absorptivity (extinction coefficient) of the acceptor at wavelength λ in M^{-1} cm^{-1}. For HSA, K^2, φ, and n are taken as 2/3, 0.118, and 1.33, respectively.[37] By using eq 7−9, values of J, E_{FRET}, R_o, and r are calculated and listed in Table 3. The

Table 3. Steady State and Time-Resolved Fluorescence FRET Parameters

		steady state`		time resolved	
J (M^{-1} cm^{-1} nm^4)	R_o (nm)	r (nm)	E_{FRET}	r (nm)	E_{FRET}
2.45×10^{13}	1.93	2.02	0.43	2.97	0.07

overlap spectra of normalized fluorescence intensity of donor (Trp214 of HSA) emission and acceptor absorption is shown in Figure 3. The binding distance (r) obtained for the system is found to be 2.02 nm. However, it must be mentioned here that if FRET is done by steady state measurements, then the value of E_{FRET} is overestimated as steady state measurements have a contribution from static quenching, which also seems to be the principal reason for lowering the HSA fluorescence emission in the presence of FUR. Hence, to have a better understanding of exclusive FRET, we have characterized HSA-FUR system by time-resolved fluorescence measurements.

3.3. Time-Resolved Fluorescence Quenching Measurements. Fluorescence lifetime measurement serves as an indicator for exploring the local environment around fluorophores and so can be implicated to understand the interaction between drug and protein.[39] At neutral pH in aqueous solution, Trp exhibits multiple exponential decay, which has been attributed to the existence of rotamers

dx.doi.org/10.1021/jp3069877 | J. Phys. Chem. B XXXX, XXX, XXX−XXX

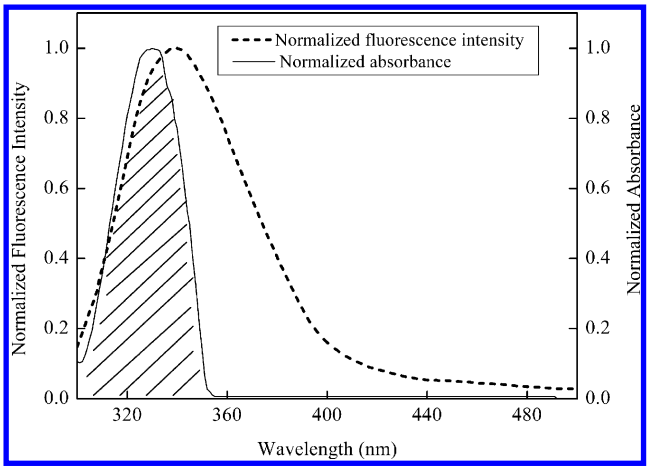

Figure 3. Overlap spectra of normalized absorbance of FUR (solid) and normalized fluorescence intensity of HSA (dashed). Equimolar (5 μM) concentration of drug and protein were taken.

(conformational isomers) in determining lifetimes.[28] The time-resolved decay profile of HSA in buffer and in the presence of FUR are displayed in Figure 4. All the experimental decay

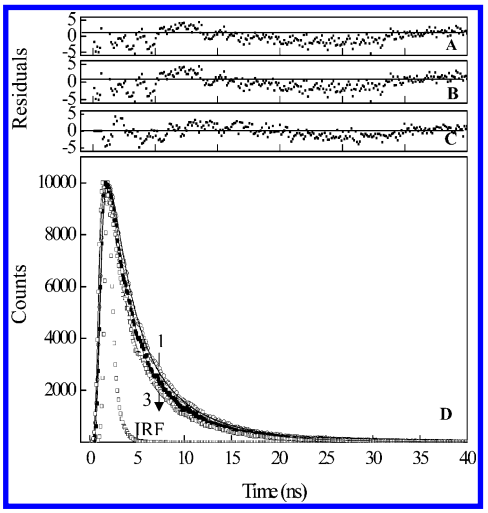

Figure 4. Time-resolved fluorescence decay profile of HSA in the absence and presence of FUR. Panels A–C show the distribution of weighted residuals for biexponential fitting for 1:0, 1:1, and 1:2 HSA:FUR. IRF indicates the instrument response function. Panel D shows the fluorescence lifetime decay of HSA:FUR at ratio of (1)1:0, (2)1:1, and (3)1:2.

curves are well reproduced with biexponential decay function as evidenced by the statistical parameters like χ^2, which is close to 1 and distribution of weighted residuals. When the biexponential decay law is used, it is often useful to determine intensity-averaged lifetime (τ_{avg}) from the deacy times (τ) and pre-exponential factors (α_1 and α_2) using[40]

$$\tau_{avg} = \frac{\alpha_1\tau_1^2 + \alpha_2\tau_2^2}{\alpha_1\tau_1 + \alpha_2\tau_2} \quad (10)$$

The intensity-averaged lifetimes (τ_{avg}) obtained are compared with those calculated by amplitude-averaged lifetime method (data not shown) using[41]

$$\langle\tau_{avg}\rangle = \alpha_1\tau_1 + \alpha_2\tau_2 \quad (11)$$

Although differences are observed in values of τ_{avg} and $\langle\tau_{avg}\rangle$, they are acceptable as reported in literature.[41−43] The τ_{avg} of HSA is found to be 5.7 ns, which decreases marginally even in the presence of a saturating concentration of FUR, as shown in Figure 4 and Table 4. This is due to the charge transfer process

Table 4. Time-Resolved Fluorescence Decay Parameters of HSA in the Presence of FUR

HSA:FUR	α_1	τ_1 (ns)	α_2	τ_2 (ns)	τ_{avg} (ns)
1:0	0.39	2.17	0.61	6.45	5.70
1:1	0.40	1.80	0.60	6.13	5.41
1:2	0.46	1.86	0.54	6.18	5.29

from the indole ring of Trp214 to the nearby substituent, which slightly enhances on binding with FUR and thus causes a slight decrease in the fluorescence lifetime. It is indicative of a small contribution of dynamic quenching as only those molecules that suffer dynamic quenching have an exclusive contribution in the decrease of the fluorescence lifetime.[44] Thus, the time-resolved transfer efficiency (E) calculated from fluorescence lifetime measurements exclusively reports the energy transfer during the process of dynamic quenching and is obtained by using the following equation:

$$E = 1 - \frac{\tau}{\tau_o} \quad (12)$$

where τ and τ_o are the lifetime of Trp in the presence and absence of FUR, respectively. Table 3 represents the FRET parameters obtained from steady state and time-resolved measurements. The magnitudes of E_{FRET} estimated from time-resolved lifetime measurements are found to be much lower than the value obtained by steady state measurements because of the exclusive contribution of dynamic quenching in the former. Thus it can be said that the mechanism of FRET is indeed operational but the magnitude of transfer efficiency is small.

3.4. Isothermal Titration Calorimetric Measurements.

ITC allows the measurement of the magnitude of binding affinity, and the two contributing thermodynamic terms: enthalpy (ΔH) and entropy (ΔS) changes. A representative calorimetric titration profile of the binding of FUR to HSA at 25, 30, and 37 °C is shown in Figure 5A–C. In the top panel, each peak represents a single injection of the drug into protein solution. The bottom panel shows an integrated plot of the amount of heat liberated per injection as a function of the molar ratio of the drug to protein. Association constant (K_b) and enthalpy change (ΔH) were directly obtained after fitting whereas free energy change is calculated from eq 6. The entropy change is calculated by

$$\Delta G = \Delta H - T\Delta S \quad (13)$$

and change in specific heat capacity can be calculated from[45]

$$\Delta C_p^{exp} = \frac{d\Delta H}{dT} \quad (14)$$

Further the van't Hoff enthalpy (ΔH_{vH}) at each temperature is calculated with

dx.doi.org/10.1021/jp3069877 | J. Phys. Chem. B XXXX, XXX, XXX−XXX

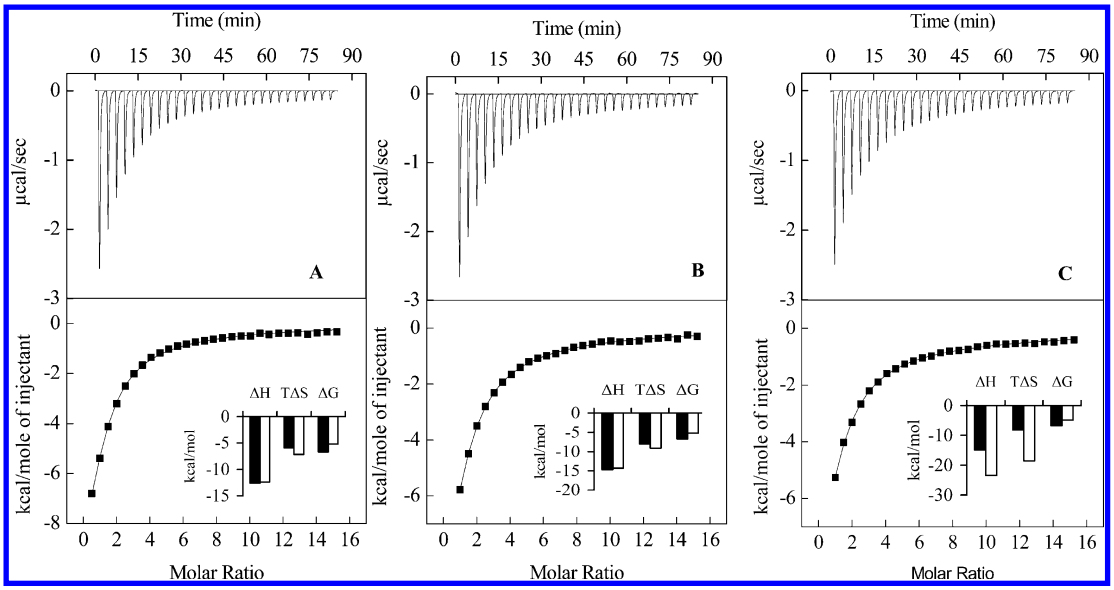

Figure 5. Isothermal titration calorimetry of HSA and FUR interaction at different temperatures. (A)−(C) represent ITC profiles of HSA-FUR system at 25, 30, and 37 °C, respectively. Titration of FUR with (18 μM) HSA at pH 7.4 shows calorimetric response as successive injections of ligand is added to the sample cell. The solid line represents the best nonlinear least-squares fit of sequential model of two binding site. The insets of (A)−(C) represent comparative bar distribution of ΔH, ΔS, and ΔG at high (filled bar) and low (open bar) affinity binding site.

Table 5. Thermodynamic Parameters and Association Constant of FUR-HSA Obtained by ITC

	Temp (°C)	K_b (M^{-1})	ΔH (kcal mol^{-1})	$T\Delta S$ (kcal mol^{-1})	ΔG (kcal mol^{-1})
high affinity site	25	$8.24 \times 10^4 \pm 4.50 \times 10^3$	−12.61 ± 0.29	−5.91	−6.70
	30	$7.03 \times 10^4 \pm 2.50 \times 10^3$	−14.74 ± 0.24	−8.03	−6.71
	37	$5.58 \times 10^4 \pm 1.20 \times 10^3$	−14.91 ± 0.15	−8.18	−6.73
low affinity site	25	$6.47 \times 10^3 \pm 4.10 \times 10^2$	−12.37 ± 0.55	−7.18	−5.19
	30	$6.21 \times 10^3 \pm 2.40 \times 10^2$	−14.34 ± 0.42	−9.09	−5.25
	37	$2.76 \times 10^3 \pm 1.10 \times 10^2$	−23.40 ± 0.72	−18.52	−4.88

$$\Delta H_{vH} = \left[\frac{\left\{ \ln \frac{K(T_2)}{K(T_1)} - \frac{\Delta C_p}{R} \ln \frac{T_2}{T_1} + \frac{\Delta C_p T_1}{R} \left(\frac{1}{T_1} - \frac{1}{T_2} \right) \right\} \times R}{\left(\frac{1}{T_1} - \frac{1}{T_2} \right)} \right] \quad (15)$$

Here, $K(T_1)$ and $K(T_2)$ are the values of binding constant at temperatures T_1 and T_2, respectively. The temperature dependency of the thermodynamic binding parameters of FUR to HSA is summarized in Table 5. The titration of FUR to HSA results in negative heat deflection at all studied temperatures, indicating that the binding is an exothermic process (Figure 5). Because albumin can bind ligand at multiple binding sites, we fit the data for two sites by the sequential binding model. The values of binding constant obtained are of the order of 10^4 and 10^3 and thus can be referred as high and low affinity sites, respectively, at each studied temperature. However, the binding constants for both types of binding sites decrease with an increase in temperature, indicating the formation of FUR-HSA complex. Besides, it is observed that at both sites of HSA, a strong dependence of ΔH and $T\Delta S$ exists with temperature whereas ΔG is insensitive to it (Table 5). As evident from the value of ΔH and ΔS, the binding becomes more exothermic with a rise in temperature, though it is entropically opposed. The negative ΔH and ΔS values at all studied temperatures suggest the involvement of hydrogen bonding in a HSA-FUR complex formation.[31] Furthermore, the plot between ΔH vs $T\Delta S$ at high and low affinity sites shows the slope of 1.02 and 0.99, respectively, which indicates the enthalpy−entropy compensation effect in which enthalpy gain due to the formation of H-bond is counterbalanced by entropic penalty due to the burial of involved groups. This effect is common in protein−ligand interactions.[46] Almost linear dependency of the ΔH with the temperature was observed in an examined range of temperature, whose slope was used to determine the change in heat capacity (ΔC_p). The values of ΔC_p were −0.18 ± 0.11 and −0.94 ± 0.24 kcal mol^{-1} $°C^{-1}$ for high and low affinity sites, respectively. The negative value of ΔC_p is suggestive of specific binding accompanied by the burial of nonpolar residues.[47] The results of ITC were in agreement with that of fluorescence spectroscopy. However, variation in magnitude of binding affinity and thermodynamic parameters was observed, which may be due to the fact that the calorimetric analysis measures a global change in property of the system whereas spectroscopic analysis measures local changes around the fluorophores/chromophores associated with the optical transition.[48,49] The binding stoichiometry obtained from spectroscopy and calorimetry was also different, which may be due to a photophysical problem because of the presence of single Trp214 in HSA.[26] Further, using eq 15 and data presented in Table 5, it is observed that the values of calorimetric enthalpies do not agree well with the van't Hoff enthalpy calculated at all studied temperatures. It indicates linkage of contribution of displacement of solvent ions and conformational changes with the binding process, which may be induced either by ligand binding or by an increase in

dx.doi.org/10.1021/jp3069877 | J. Phys. Chem. B XXXX, XXX, XXX−XXX

temperature.[48] This observation is further supported by non linear van't Hoff plot between temperature and ln K, which is also an important indication of conformational alterations linked to the binding process. So, FTIR and far-UV CD measurements are performed to monitor the secondary structure alteration on FUR binding.

3.5. Circular Dichroism Measurements. To monitor the secondary structural change of protein upon interaction with FUR, we perform far UV circular dichroism. The results are expressed as MRE (mean residue ellipticity) in deg cm^2 dmol^{-1}, which is given by

$$\mathrm{MRE} = \frac{\Theta_{\mathrm{obs}}\,(\mathrm{mdeg})}{10 \times n \times c \times l} \tag{16}$$

where θ_{obs} is the observed ellipticity in millidegrees, c is the concentration of protein in mol/L, l is the length of the light path in centimeters, and n is the number of peptide bonds. Panels A–C of Figure 6 show the far-UV CD spectra of HSA in

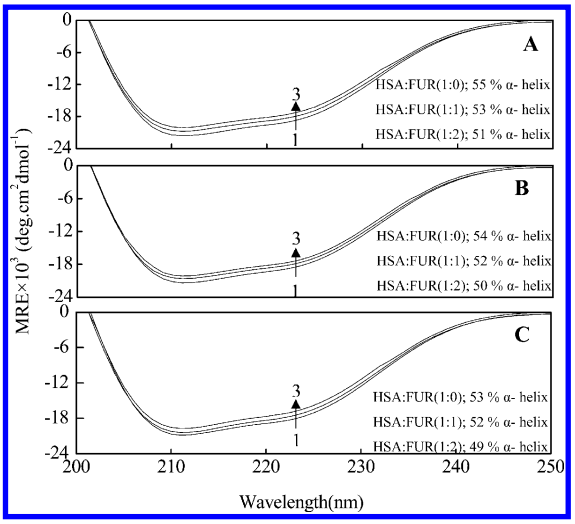

Figure 6. Circular dichroism spectra of HSA (5 μM) in the presence of FUR at ratios of (1) 1:0, (2) 1:1, and (3) 1:2 at (A) 25 °C, (B) 30 °C, and (C) 37 °C.

the absence and presence of FUR at 25, 30, and 37 °C, respectively. The far-UV CD spectra of HSA exhibit two negative bands at 208 and 222 nm, which is characteristic of the typical α-helix structure of protein.[26,27] Furthermore, to investigate the change in percent α helical structure of HSA on addition of FUR, we analyze CD data by the method of Chen et al.[50]

$$\%\ \alpha\text{-helix} = \left(\frac{\mathrm{MRE}_{222\mathrm{nm}} - 2340}{30300}\right) \times 100 \tag{17}$$

The estimated percent α-helical content in free HSA is 55, 54, and 53% at 25, 30, and 37 °C, respectively, which is in reasonable accord with the available literature.[26,27,51] The data compiled in the inset of Figure 6A–C indicate the slight decrease in α-helical content on addition of FUR in ratios of 1:1 and 1:2 (HSA:FUR) at all studied temperatures. The observed decrease in percent α-helical content might be induced by the formation of the FUR–HSA complex. However, the shape of peaks and the position of peak maximum remain almost unchanged in the presence and absence of FUR, indicating that HSA is predominantly α-helix in nature even after binding to the drug.

3.6. FTIR Spectroscopic Measurements. Band frequencies due to amide I, II, and III vibrations in the IR region are sensitive to the secondary structure of protein. But, generally, amide I (1700–1600 cm^{-1}) is analyzed to investigate the change in secondary structure of protein as it reflects C═O stretching vibration of the amide group weakly coupled with in plane NH bending and CN stretching.[52] Figure S1 (Supporting Information) shows the fitted curve of HSA and HSA-FUR complex in a molar ratio of 1:1. The free HSA has 54% α-helix, 18% β-sheet, 4% β-antiparallel, 11% disordered, and 13% turn, which is reasonable accord with the literature.[53] From Figure S1, it can be seen that there is not much difference in position of the amide I components, but their intensities differ. So, from quantitative analysis of the amide I band, it was observed that amount of α-helix decreases on HSA-FUR complex formation, which agrees with far-UV CD results.

3.7. Effect of Drug Binding on Esterase-Like Activity of HSA. The Arg410 and Tyr411 present in the center of drug binding site II of HSA are the two crucial amino acid residues involved in esterase-like activity.[24] Thus, esterase-like activity of HSA using p-nitrophenyl acetate as the substrate is investigated in the presence and absence of FUR to know the involvement of Arg410 and Tyr411 in FUR binding. Kinetic constants are obtained using Graph-Pad Prism, version 5.0, software by fitting the initial rates to Michaelis–Menten equation:

$$v = \frac{V_{\mathrm{max}}[\mathrm{S}]}{K_{\mathrm{m}} + [\mathrm{S}]} \tag{18}$$

where v, V_{max}, K_{m}, and [S] represent the initial reaction velocity, maximum velocity, Michaelis–Menten constant, and molar concentration of substrate, respectively. Further, K_{i} is calculated from

$$K'_{\mathrm{m}} = \frac{K_{\mathrm{m}}}{K_{\mathrm{i}}} I_{\mathrm{o}} + K_{\mathrm{m}} \tag{19}$$

where K'_{m} is the apparent K_{m} in the presence of competitive inhibitor concentration I_{o}. Figure 7 shows the Michaelis–Menten and double reciprocal plot in the absence and presence

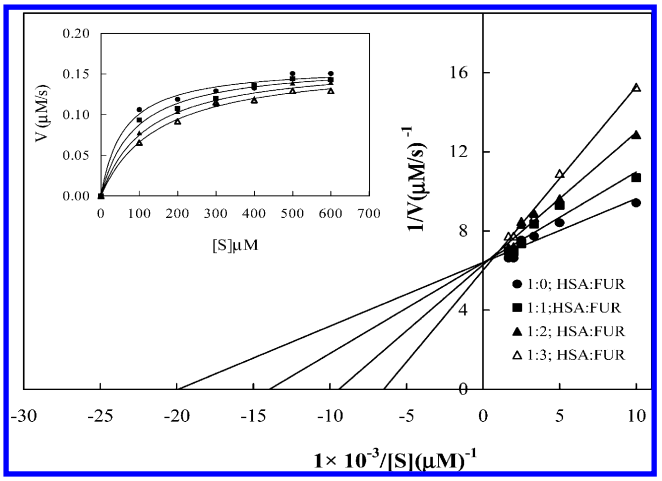

Figure 7. Plot between $1/V$ and $1/[\mathrm{S}]$ of esterase-like activity of HSA in varying concentration of FUR (inhibitor). The inset shows the Michaelis–Menten plot of HSA for p-NPA under same condition. The effect of varying concentration of FUR on the apparent K_{m} for p-NPA(S) is examined in 20 mM sodium phosphate, pH 7.4 at 25 °C. HSA (15 μM) and HSA:FUR ratios of 1:0, 1:1, 1:2, and 1:3 are used.

dx.doi.org/10.1021/jp3069877 | J. Phys. Chem. B XXXX, XXX, XXX–XXX

of different drug to HSA molar ratios. HSA acts as esterase toward *p*-NPA and shows K_m and V_{max} equals 59.36 μM and 0.16 μM s^{-1}, respectively (Table 6), which remain similar even

Table 6. Kinetic Parameters for the Hydrolysis of *p*-NPA by HSA

HSA:FUR	K_m (μM)	V_{max} (μMs^{-1})	$10^5 \times k_{cat}/K_m$ ($\mu M^{-1}s^{-1}$)
1:0	59.36 ± 05.55	0.16 ± 0.01	17.95
1:0.5	60.12 ± 05.52	0.16 ± 0.01	17.73
1:1	86.60 ± 06.47	0.16 ± 0.02	12.30
1:2	120.40 ± 09.42	0.16 ± 0.01	08.85
1:3	149.60 ± 10.67	0.16 ± 0.02	07.12

in the presence of a FUR to HSA ratio of 0.5. However, on a further increase in the ratio of FUR to HSA, there occurs inhibition of activity in a competitive manner with K_i equal to 28.72 μM; i.e., K_m changes while V_{max} remains nearly unaltered, as shown in Figure 7 and Table 6. Because FUR has drug site I as a high affinity site up to a FUR to HSA ratio of 0.5, the drug binds mainly to site I on HSA and thus no changes occur in K_m, V_{max}, and k_{cat}/K_m ratio. But on a further increase in FUR concentration over HSA, the drug starts binding to its low affinity site, which has Arg410 and Tyr411 amino acid residues, and thus competitively inhibits esterase-like activity of HSA and hence a decrease in catalytic efficiency is observed. This confirms the involvement of these amino acids in FUR binding to HSA.

3.8. Molecular Docking Studies of FUR-HSA Interaction. The binding sites of FUR on HSA are located by using the docking software GLIDE.[25] Figure 8A,B and Table 7 represent the involvement of crucial amino acid residues in the binding of FUR to the two different sites on HSA. The residues that overlap with specific site markers of site I (i.e., PBZ, WAR) and site II (DIA) are also shown. According to the GLIDE score, the FUR fit most favorably in site I of HSA with GLIDE and X-score of −7.32 and −7.99 kcal mol^{-1}, respectively. Figure 8D and Table 7 show that at site I, FUR hydrophobically interacts with Ala291, Leu238, Lys195, Tyr150, and Trp214 whereas O1, O4, and N1 groups involved in hydrogen bonding with the NH_2 group of Lys199 of HSA with bond length of 3.10, 2.69, and 2.98 Å, respectively. The two side chain NH_2 groups of Arg222 also interact with O5 of FUR having hydrogen bond length of 2.85 and 2.66 Å. However, FUR also binds to a site that is in the vicinity of site II of HSA with GLIDE and X-score of −5.53 and 6.89 kcal mol^{-1}, respectively. This site shares some of the amino acid residues of site II like Arg410, Lys414, Ser489, and Glu492. The NH_2 group of the side chain of Arg410 and Lys414 and OH of carboxylate group of Glu492 of HSA interact with O1, O5, and O2 of FUR with hydrogen bond lengths of 3.24, 2.62, and 2.66 Å, respectively. Moreover, FUR interacts hydrophobically with Lys413, Gln390, Leu394, Ala406, Val493, and others (Figure 8C). Panels E and F of Figure 8 show the molecular surface representation of FUR in the binding pockets of HSA. Thus FUR has drug binding site I as the high affinity binding site whereas a new site that shares Arg410 and some other amino acid residues like Lys414 and Ser489 has site II as the low affinity binding site. Further, it is also established that FUR-HSA binding involves hydrogen bonding and hydrophobic interaction as the main binding forces.

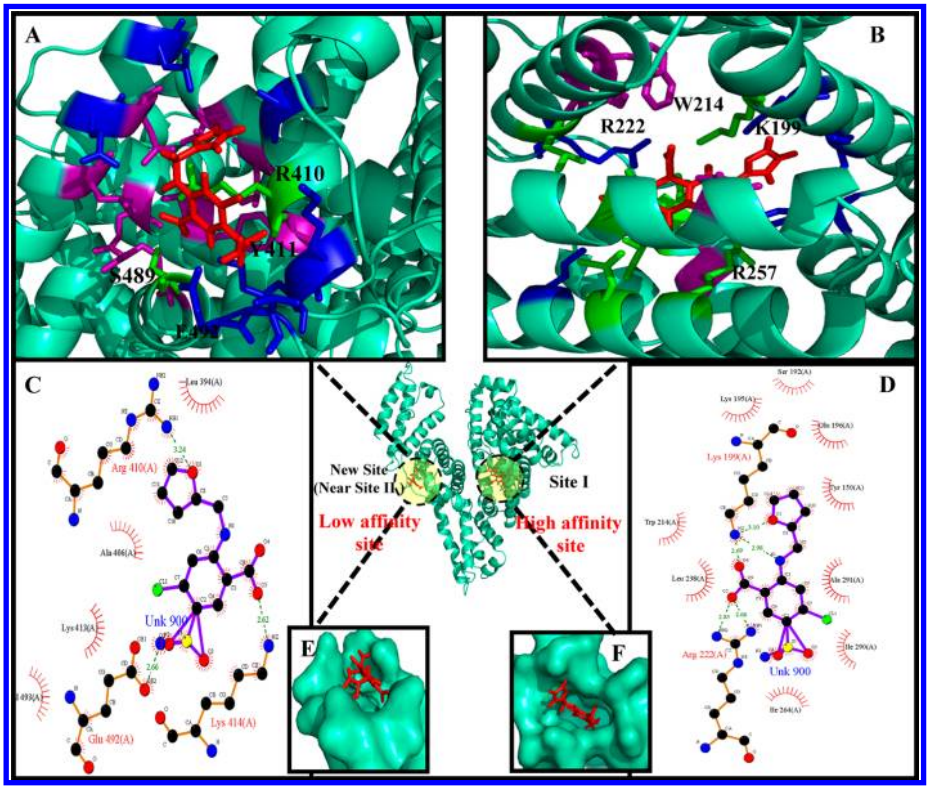

Figure 8. Molecular docking of FUR with HSA: Cartoon representation of docked FUR in a site I (A) of HSA and new site near site II (B). Residue interacting with FUR only (blue), PBZ and DIA only (purple), and common to FUR, PBZ, or DIA (green). Lig plots of new site (C) and site I (D), respectively. Molecular surface representation of new site (E) and site I (F).

dx.doi.org/10.1021/jp3069877 | J. Phys. Chem. B XXXX, XXX, XXX−XXX

Table 7. Results of Docking of HSA with FUR Obtained from GLIDE Docking Software

binding site	amino acid	ΔASA (Å^2)	forces involved	GLIDE score (kcal mol^{-1})	X-score (kcal mol^{-1})	−log(K_d)	no. of other residue (5 Å)
site I	Ala291	36.67	hydrophobic interaction	−7.32	−7.99	5.86	5
	Leu238	30.27	hydrophobic interaction				
	Lys199	21.96	hydrogen bonding [*Lys199-NH_2---O═C FUR(2.69 Å) *Lys199-NH_2----NH FUR(2.98 Å) *Lys199-NH_2---O═C FUR(3.10 Å)]				
	Arg222	19.00	hydrogen bonding [*Arg222-NH_2---O═C FUR(2.85 Å) *Arg222-NH_2---O═C FUR(2.66 Å)]				
	Lys195	16.10	hydrophobic interaction				
	Tyr150	15.80	hydrophobic interaction				
	Arg257	14.13	hydrophobic interaction				
	Ile290	13.03	hydrophobic interaction				
	Leu260	12.65	hydrophobic interaction				
	Leu219	12.53	hydrophobic interaction				
	Ile264	10.89	hydrophobic interaction				
	Ser192	10.35	hydrophobic interaction				
new site	Arg410	64.43	hydrogen bonding [*Arg-410-NH_2---O═C FUR(3.24 Å)	−5.53	−6.89	5.05	
(near site II)	Glu492	30.83	*Glu-492 -C═O---NH_2 FUR(2.66 Å)]				
	Lys413	24.55	hydrophobic interaction				
	Gln390	19.31	hydrophobic interaction				
	Leu394	15.17	hydrophobic interaction				
	Ala406	14.80	hydrophobic interaction				
	Lys414	13.38	hydrogen bonding [*Lys-414-NH_2---O═C FUR(2.62 Å)]				
	Val493	11.66	hydrophobic interaction				
	Ser489	10.12	hydrophobic interaction				

3.9. Correlation between Binding Sites of FUR and Uremic Toxins. To account for the mechanisms that govern inhibition of FUR binding to HSA in uremia, we carefully examine the relationship between the FUR and the uremic toxin binding sites. From the above studies, it is found that the FUR primarily binds to site I of HSA and binds with relatively low affinity to a site having some crucial residues (Arg410, Lys414, and Ser489) of site II. However, available literature[19−21] suggests that uremic toxins like IS, IAA, and HA bind mainly to site II whereas CMPF binds to site I of HSA. Thus, these findings suggest that FUR competes directly with site I bound uremic toxins (CMPF) but indirectly competes with site II bound uremic toxins (IA, IS, HA) for some residue, as shown in Figure 9.

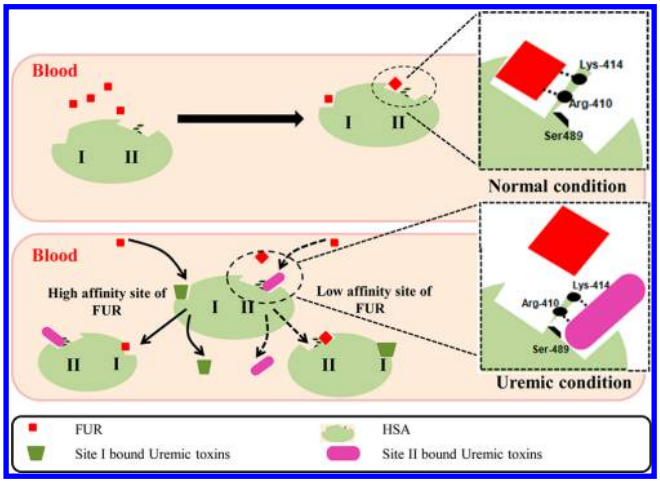

Figure 9. Schematic representation of mechanism of FUR binding to HSA under normal and uremic condition.

4. CONCLUSIONS

In this study, the mechanism of impaired binding of FUR to HSA in uremia is uncovered by determining binding energetic and binding sites of FUR on HSA. Results indicate that the quenching mechanism of fluorescence of HSA by FUR is a static procedure and their binding is a spontaneous, enthalpically driven, entropically opposed process that involves both hydrogen bonding and hydrophobic interaction. Moreover, FUR strongly binds to site I of HSA and with relatively low affinity to a site having some crucial amino acid residue like Arg410 and Lys414 and Ser489 of site II. Thus it directly competes with the site I bound uremic toxins (CMPF) and indirectly competes with site II bound uremic toxins (IA, IS, HA). Furthermore, our study can also be helpful to explicate the reason behind impaired albumin binding of all those drugs which possess similar binding sites.

■ ASSOCIATED CONTENT

Supporting Information

Figures obtained from FTIR measurements for the determination of secondary structures of free HSA and FUR-bound HSA. This information is available free of charge via the Internet at http://pubs.acs.org.

dx.doi.org/10.1021/jp3069877 | J. Phys. Chem. B XXXX, XXX, XXX−XXX

AUTHOR INFORMATION

Corresponding Author

*E-mail: rizwanhkhan@hotmail.com, rizwanhkhan1@gmail.com. Fax: + 91-571-2721776. Tel.: +91-571-2720388.

Notes

The authors declare no competing financial interest.

ACKNOWLEDGMENTS

The Council of Scientific and Industrial Research (CSIR), New Delhi, India, has been acknowledged for providing financial assistance in the form of Senior Research Fellowship (SRF) to N.Z. The comments of reviewers that enabled us to improve manuscript are also highly appreciated.

REFERENCES

(1) Varshney, A.; Sen, P.; Ahmad, E.; Rehan, M.; Subbarao, N.; Khan, R. H. *Chirality* **2010**, *22*, 77−87.

(2) Kragh-Hansen, U. *Pharmacol. Rev.* **1981**, *33*, 17−53.

(3) Peters, T. Jr. *All about Albumin: Biochemistry, Genetics, and Medical Applications*; Academic Press: San Diego, CA, 1996.

(4) He, X. M.; Carter, D. C. *Nature* **1992**, *358*, 209−215.

(5) Sugio, S.; Mochizuki, S.; Noda, M.; Kashima, A. *Protein Eng.* **1999**, *12*, 439−446.

(6) Sudlow, G.; Birkett, D. J.; Wade, D. N. *Mol. Pharmacol.* **1975**, *11*, 824−832.

(7) Kamat, B. P.; Seetharamappa, J. *J. Pharma. Biomed. Anal.* **2005**, *39*, 1046−1050.

(8) Reed, M. D.; Myers, C. M.; Blumer, J. L. *Curr. Ther. Res.* **2001**, *8*, 558−565.

(9) Varshney, A.; Rehan, M.; Subbarao, N.; Rabbani, G.; Khan, R. H. *PLoS ONE* **2011**, *6*, e17230.

(10) Mingrone, G.; Smet, R.; Greco, A.; Bertuzzi, A.; Gandel, A. *Clin. Chim. Acta* **1997**, *260*, 27−34.

(11) Bojko, B.; Sułkowska, A.; Maciazek-Jurczyk, M.; Równicka, J.; Pentak, D.; Sułkowski, W. W. *J. Pharm. Biomed. Anal.* **2010**, *51*, 273−277.

(12) Takamura, N.; Maruyama, T.; Chosa, E.; Kawai, K.; Tsutsumi, Y.; Uryu, Y.; Yamasaki, K.; Deguchi, T.; Otagiri, M. *Drug Metab. Dispos.* **2005**, *33*, 596−602.

(13) Christopher, S.; Wilcox. *J. Am. Soc. Nephrol.* **2002**, *13*, 798−805.

(14) Sjoholm, I.; Kober, A.; Odar-Cederlof, I.; Borga, O. *Biochem. Pharmacol.* **1976**, *25*, 1205−1213.

(15) Takamura, N.; Haruta, A.; Kodama, H.; Tsuruoka, M.; Yamasaki, K.; Suenaga, A.; Otagiri, M. *Pharam. Res.* **1996**, *13*, 1015−1019.

(16) Ivanov, A. I.; Korolenko, E. A.; Korolik, E. V.; Firsov, S. P.; Zhbankov, R. G.; Marchewka, M. K.; Ratajczak, H. *Arch. Biochem. Biophys.* **2002**, *408*, 69−77.

(17) Sarnatskaya, V. V.; Lindup, W. E.; Ivanov, A. I.; Yushko, L. A.; Tjia, J.; Maslenny, V. N.; Gurina, N. M.; Nikolaev, V. G. *Nephron. Physiol.* **2003**, *95*, 10−18.

(18) Bojko, B.; Sułkowska, A.; Maciazek-Jurczyk, M.; Równicka, J.; Sułkowski, W. W. *Spectrochim. Acta A Mol. Biomol. Spectrosc.* **2010**, *76*, 6−11.

(19) Bowmer, C. J.; Lindup, W. E. *Biochem. Pharmacol.* **1982**, *31*, 319−23.

(20) Ikeda, K.; Yoshitomi, H.; Nakayama, T.; Goto, S.; Kimura, T. *J. Pharm. Pharmacol.* **1984**, *36*, 663−667.

(21) Sakai, T.; Takadate, A.; Otagiri, M. *Biol. Pharm. Bull.* **1995**, *18*, 1755−1761.

(22) Lakowicz, J. R. *Principles of Fluorescence Spectroscopy*, 3rd ed.; Plenum: New York, USA, 2006; pp 54−57.

(23) Barth, A. *Biochim. Biophys. Acta* **2007**, *1767*, 1073−1101.

(24) Watanabe, H.; Tanase, S.; Nakajou, K.; Maruyama, T.; Kragh-Hansen, U.; Otagiri, M. *Biochem. J.* **2000**, *349*, 813−819.

(25) Friesner, R. A.; Banks, J. L.; Murphy, R. B.; Halgren, T. A.; Klicic, J. J.; Mainz, D. T.; Repasky, M. P.; Knoll, E. H.; Shelley, M.; Perry, J. K.; Shaw, D. E.; Francis, P.; Shenkin, P. S. *J. Med. Chem.* **2004**, *47*, 1739−1749.

(26) Ahmad, E.; Rabbani, G.; Zaidi, N.; Singh, S.; Rehan, M.; Khan, M. M; Rahman, S. H.; Quadri, Z.; Shadab, M.; Ashraf, M. T.; Subbarao, N.; Bhat, R.; Khan, R. H. *PLoS ONE* **2011**, *6*, e 26186.

(27) Ahmad, B.; Parveen, S.; Khan, R. H. *Biomacromolecules* **2006**, *7*, 1350−1356.

(28) Anand, U.; Jash, C.; Boddepalli, R. K.; Shrivastava, A.; Mukherjee, S. *J. Phys. Chem. B* **2011**, *115*, 6312−6320.

(29) Lakowicz, J. R. *Principles of Fluorescence Spectroscopy*, 2nd ed.; Plenum: New York, USA,1999; pp 277−283.

(30) Ibrahim, N.; Ibrahim, H.; Kim, S.; Nallet, J. P.; Nepveu, F. *Biomacromolecules* **2010**, *11*, 3341−3351.

(31) Chi, Z.; Liu, R. *Biomacromolecules* **2011**, *12*, 203−209.

(32) Ross, P. D.; Subramanian, S. *Biochemistry* **1981**, *20*, 3096−3102.

(33) Petipas, I.; Bhattacharya, A. A.; Twine, S.; East, M.; Curry, S. *J. Biol. Chem.* **2001**, *276*, 22804−22809.

(34) Ghuman, J.; Zunszain, P. A.; Petitpas, I.; Bhattacharya, A. A.; Otagiri, M.; Curry, S. *J. Mol. Biol.* **2005**, *353*, 38−52.

(35) Förster, T. *Ann. Phys. 2* **1948**, *473*, 55−75.

(36) Il'ichev, Y. V.; Perry, J. L.; Simon, J. D. *J. Phys. Chem. B* **2002**, *106*, 452−459.

(37) Cyril, L.; Earl, J. K.; Sperry, W. M. *Biochemists' Handbook*; E. & F. N. Spon: London, 1961.

(38) Hu, Y. J.; Liu, Y.; Xiao, X. H. *Biomacromolecules* **2009**, *10*, 517−521.

(39) Anand, U.; Jash, C.; Mukherjee, S. *J. Phys. Chem. B* **2010**, *114*, 15839−15845.

(40) Lakowicz, J. R. *Principles of Fluorescence Spectroscopy*, 2nd ed.; Plenum: New York, USA,1999; pp 141−142.

(41) Kelkar, D. A.; Chattopadhyay, A.; Chakrabarti, A.; Bhattacharyya, A. *Biopolymers* **2005**, *77*, 325−334.

(42) Haldar, S.; Chaudhari, A.; Gu, H.; Koeppe, R. E.; Kombrabail, M.; Krishnamoorthy, G.; Chattopadhyay, A. *J. Phys. Chem. B* **2012**, *116*, 11056−11064.

(43) Haldar, A.; Raghuraman, H.; Chattopadhyay, A. *J. Phys. Chem. B* **2008**, *112*, 14075−14082.

(44) Beechem, J. M.; Brand, L. *Annu. Rev. Biochem.* **1985**, *54*, 43−71.

(45) Williams, M. A.; Ladbury, J. E. *Curr. Opin. Struct. Biol.* **2004**, *14*, 562−569.

(46) Zolotnitsky, G.; Cogan, U.; Adir, N.; Solomon, V.; Shoham, G.; Shoham, Y. *Proc. Natl. Acad. Sci. U. S. A.* **2004**, *101*, 11275−11280.

(47) Kumaran, S.; Jez, J. M. *Biochemistry* **2007**, *46*, 5586−5594.

(48) Faergeman, N. J.; Sigurskjold, B. W.; Kragelund, B. B.; Anderson, K. V.; Knudsen, J. *Biochemistry* **1996**, *35*, 14118−14126.

(49) Nada, T.; Terazima, M. *Biophys. J.* **2003**, *85*, 1876−1881.

(50) Chen, Y. H.; Yang, J. T.; Martinez, H. *Biochemistry* **1972**, *11*, 4120−4131.

(51) Beauchemin, R.; N'soukpoé-Kossi, C. N.; Thomas, T. J.; Thomas, T.; Carpentier, R.; Tajmir-Riahi, H. A. *Biomacromolecules* **2007**, *8*, 3177−3183.

(52) Tian, J.; Liu, J.; He, W.; Hu, Z.; Yao, X.; Chen, X. *Biomacromolecules* **2004**, *5*, 1956−1961.

(53) Froehlich, E.; Mandeville, J. S.; Jennings, C. J.; Sedaghat-Herati, R.; Tajmir-Riahi, H. A. *J. Phys. Chem. B* **2009**, *113*, 6986−6993.